

Supplementary information for Fast Accurate State Measurement with Superconducting Qubits

Evan Jeffrey,* Daniel Sank,* J.Y. Mutus, T.C. White, J. Kelly, R. Barends, Y. Chen, Z. Chen, B. Chiaro, A. Dunsworth, A. Megrant, P.J.J. O'Malley, C. Neill, P. Roushan, A. Vainsencher, J. Wenner, A. N. Cleland, and John M. Martinis
Department of Physics, University of California, Santa Barbara, California 93106-9530, USA

Here we present theoretical and technical details on the design of the bandpass filter and measurement resonators used in the experiment. We also describe the method used to measure the quantum efficiency of the detector. Finally we show a full diagram of the experimental set-up.

ENVIRONMENTAL LIMIT OF QUBIT COHERENCE

In this section we present analytic and numerical models of the response-lifetime product $\kappa_r T_1$. Because the qubit is nearly harmonic we can use linear circuit theory to calculate T_1 of the excited state [1] [1]. We calculate the Q of an equivalent linear circuit element and then write it in terms of T_1 using $Q_q \equiv \omega_q T_1$.

Theory

We first present an analytic calculation. A diagram of the theoretical model is shown in Fig. 1. The quality factor of the qubit Q_q is defined as

$$Q_q \equiv \frac{\text{energy stored in qubit}}{\text{energy lost per radian}}. \quad (1)$$

The energy stored in the qubit is $E_q = \frac{1}{2} C_q |V_q|^2$ where C_q is the qubit capacitance and V_q is the voltage amplitude at the qubit node as indicated in Fig. 1. Assuming that the only lossy element in the system is the filter, we use the definition of the filter quality factor Q_F to write

$$\text{energy lost per radian} = E_F / Q_F, \quad (2)$$

where $E_F = \frac{1}{2} C_F |V_F|^2$ is the energy stored in the filter. Inserting Eq. (2) into (1) yields

$$Q_q = Q_F \frac{C_q}{C_F} \left| \frac{V_q}{V_F} \right|^2, \quad (3)$$

where C_F and V_F are the filter capacitance and voltage amplitude. See Fig. 1(a). To compute the ratio V_q/V_F we use voltage division. We make the crucial observation that to calculate the qubit damping we must analyze the circuit impedances *at the qubit frequency*. Because the qubit is off resonance from the measurement resonator, the measurement resonator's impedance Z_r is lower than the impedance Z_g of the coupling capacitor C_g , ie. $Z_r \ll Z_g$. Therefore with voltage V_q across the qubit, we have a current $I_g = V_q/Z_g$ flowing through C_g . By similar reasoning $Z_r \gg Z_r$, so most of the current

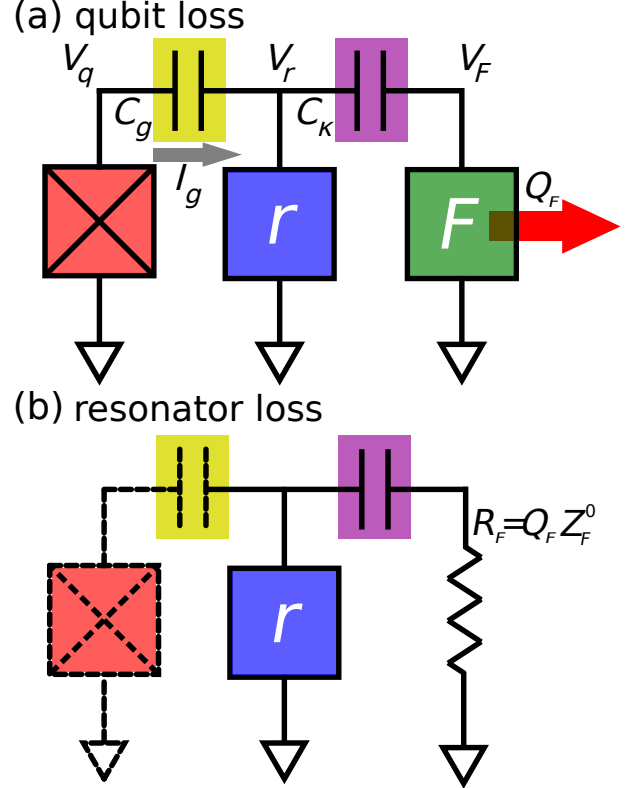


FIG. 1: (color online) Lumped element circuit model of the measurement system. The qubit (cross), measurement resonator (r), and filter (F) are connected through coupling capacitors. (a) For qubit loss we assume the filter is the only lossy element, so system energy only leaves through the finite Q_F of the filter. (b) For calculation of Q_r we work at the measurement resonator frequency. The measurement resonator and filter are on resonance, so the filter impedance is nearly real and modelled as a resistor. The qubit and coupling capacitor C_g , indicated with dotted lines, are lossless and therefore ignored.

I_g flows through the measurement resonator. This gives $V_r = I_g Z_r = V_q Z_r / Z_g$. Using similar arguments to work through each stage of the circuit we arrive at

$$\frac{V_q}{V_F} = \frac{Z_g Z_r}{Z_r Z_F}. \quad (4)$$

Note the shunt impedances in the denominator and the coupling impedances in the numerator.

Next we compute Z_r and Z_F in terms of their characteristic impedances. The impedance of a parallel harmonic mode is

$$\frac{1}{Z} = \frac{i}{Z^0} \frac{2\delta x + \delta x^2}{1 + \delta x}, \quad (5)$$

where $\delta x \equiv (\omega - \omega_0)/\omega_0$, ω_0 is the resonance frequency, and Z^0 is the characteristic impedance of the resonance (equal to $\sqrt{L/C}$ for a parallel LC). Inserting Eq. (5) into (4) we get

$$\left| \frac{V_q}{V_F} \right| = \frac{|Z_g| |Z_\kappa|}{Z_r^0 Z_F^0} \left(\frac{2\delta x + \delta x^2}{1 + \delta x} \right)^2, \quad (6)$$

where here $\delta x \equiv (\omega_q - \omega_r)/\omega_r$, ω_r is the measurement resonator frequency, and we assume the measurement resonator and filter have the same resonance frequencies. Inserting Eq. (6) into (3) yields

$$Q_q = Q_F \frac{C_q}{C_F} \left(\frac{|Z_g| |Z_\kappa|}{Z_r^0 Z_F^0} \right)^2 \left(\frac{2\delta x + \delta x^2}{1 + \delta x} \right)^4. \quad (7)$$

Equation (7) expresses Q_q in terms of circuit element values, but to produce a more useful design formula we must eliminate Z_κ in favor of Q_r . To calculate Q_r we work at the measurement resonator frequency. With the measurement resonator and filter assumed to be nearly on resonance the filter appears as a pure resistance $R_F = Q_F Z_F^0$, as shown in Fig. 1(b). We assume the qubit to be lossless so the filter resistance sets Q_r . Using a method similar to that which led to Eq(7) we find

$$Q_r = \frac{|Z_\kappa|^2}{R_F Z_r^0} = \frac{|Z_\kappa|^2}{Q_F Z_F^0 Z_r^0}. \quad (8)$$

Substituting Eq.(8) into (7) and using $Q_q = \omega_q T_1$ and $Q_r = \omega_r / \kappa_r$ we find

$$\kappa_r T_1 = Q_F^2 \left(\frac{\omega_r}{\omega_q} \right)^2 \left(\frac{C_q}{C_g} \right)^2 \frac{Z_q^0}{Z_r^0} \left(\frac{2\delta x + \delta x^2}{1 + \delta x} \right)^4. \quad (9)$$

Equation (9) is most useful when comparing with results from numerical circuit simulators and when choosing values for the actual circuit hardware. For the present experiment in which we use $\lambda/4$ resonators it is convenient to use the relation between the filter characteristic impedance and the line impedance $Z_r^0 = (4/\pi)Z_0$ resulting in

$$\kappa_r T_1 = \frac{\pi}{4} Q_F^2 \left(\frac{\omega_r}{\omega_q} \right)^2 \left(\frac{C_q}{C_g} \right)^2 \frac{Z_q^0}{Z_0} \left(\frac{2\delta x + \delta x^2}{1 + \delta x} \right)^4. \quad (10)$$

We used Eq. (10) as our design formula.

For an equation applicable to other physical systems we eliminate capacitances and impedances in favor of

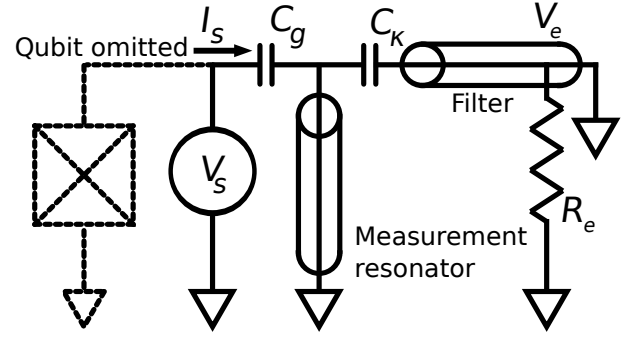


FIG. 2: Circuit model used in SPICE simulation. Elements shown in solid line were simulated. The resistor R_e models the 50Ω environment imposed by the amplification chain. The impedance of the circuit shown in solid line is measured by sourcing V_s and measuring I_s .

coupling constants. Using the standard formula for capacitive coupling between harmonic modes

$$g = \frac{1}{2} \frac{C_g}{\sqrt{C_q C_r}} \sqrt{\omega_q \omega_r}, \quad (11)$$

and keeping only the leading order in δx we can re-express Eq. (10) as

$$\kappa_r T_1 = 4 \frac{\Delta^4}{g^2 \omega_q^2 / Q_F^2} = \left(\frac{\Delta}{g} \right)^2 \left(\frac{\omega_r}{\omega_q} \frac{2\Delta}{\omega_r / Q_F} \right)^2, \quad (12)$$

where $\Delta \equiv \omega_q - \omega_r$, and ω_r / Q_F is the filter bandwidth. Equation (12) provides the link between measurement time and qubit coherence. With our design parameters $Q_F = 30$, $\Delta/2\pi = 800$ MHz, $g/2\pi = 90$ MHz, $\omega_r/2\pi = 6.8$ GHz, and $\omega_q/2\pi = 6$ GHz we get $\kappa_r T_1 = 5050$. An engineered leakage rate of $\kappa_r = 1/50$ ns gives $T_1 = 250 \mu\text{s}$. We designed our four κ_r values to range from 1/12 ns to 1/71 ns.

Numerics

We compared Eq. (10) against a numerical simulation of the circuit in SPICE [?]. The circuit model is shown in Fig. 2. The quality factor of the qubit is determined in a simple two step procedure. First, we replace the qubit with a voltage source. We activate the voltage source with an amplitude V_s at frequency ω and record the complex current I_s flowing into the rest of the circuit. The admittance of the circuit external to the qubit is then

$$Y_e(\omega) = I_s / V_s. \quad (13)$$

Second, we compute the T_1 of the qubit as [1]

$$T_1 = C_q / |\text{Re} Y_e(\omega_q)|. \quad (14)$$

Results of the simulation with corresponding predictions from Eq. (10) are shown in Fig. 3. We plot the T_1 limit

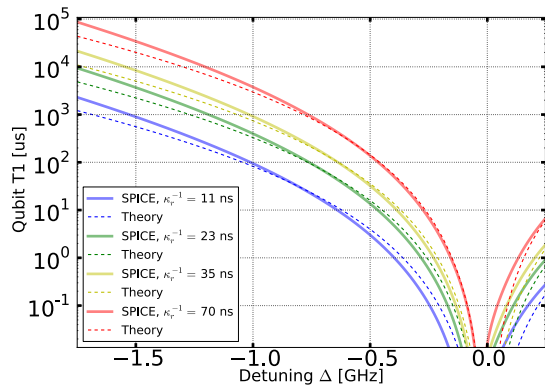


FIG. 3: (color online) Analytic (Eq. 7) and numerical (SPICE) qubit T_1 limits for several values of κ_r .

versus detuning between the qubit and measurement resonator for several values of Q_r . We note that the simple linear theory agrees very well with the numerical result up to $\Delta/(2\pi) \approx 1$ GHz. The disparity at larger detunings probably comes from the assumption, made in deriving Eq. (4), that the coupling capacitance impedances Z_g and Z_κ are much larger than the resonator impedances at the qubit frequency.

DEVICE PARAMETERS

The superconducting Xmon transmon qubits were fabricated from etched Al films on a sapphire substrate as in Ref. [2]. We include additional lithography and deposition steps to form Al on SiO_2 dielectric wire crossovers to suppress spurious modes on the chip and reduce parasitic inductances responsible for large unwanted frequency shifts in the filter resonance [3, 4]. In Table I we give the measured and target parameters for the four qubits used in the experiment. The measurement resonator ring-down time κ_r was varied across the four qubits. The qubit-resonator coupling g was adjusted for each κ_r to keep the IQ clouds corresponding to the two qubits states maximally separated.

QUANTUM EFFICIENCY

The rate of separation fidelity improvement during the equilibrium part of the measurement increases with increasing flux of detected measurement photons. Each measurement photon carries information about the qubit state and therefore incurs dephasing of the qubit [5]. This results in a direct relationship between the separation of the measured IQ clouds and the qubit phase coherence (ignoring any additional decoherence channels in the

	$\omega_r/2\pi$ [GHz]	$g/2\pi$ [MHz]	$1/\kappa_r$ [ns]
Q_1	6.835 (6.805)	100 (146)	19 (12)
Q_2	6.789 (6.765)	86 (102)	37 (23)
Q_3	6.848 (6.735)	76 (84)	50 (35)
Q_4	6.737 (6.705)	50 (59)	147 (71)

TABLE I: Parameters for the four qubits. Each was designed with a different target κ_r in order to test the tradeoff between damping and measurement speed. Target design values are given in parentheses. Disparity between target and measured values probably comes from errors in predicting in-plane capacitances between structures.

qubit)

$$|\rho_{10}| = \exp\left[-\frac{s^2}{8\sigma^2}\right]. \quad (15)$$

Here ρ_{10} is the amplitude of the off-diagonal elements of the qubit density matrix, s is the distance between the centers of the $|0\rangle$ and $|1\rangle$ IQ clouds, and σ is their widths (assumed to be equal). Equation (15) provides a means of determining the fraction of photons lost to dissipation in the measurement system. Lost photons decohere the qubit, but do not contribute to the separation of the IQ clouds. Therefore, by measuring the cloud separation and the dephasing induced on the qubit, we can extract the fraction of photons lost in the measurement process. We found a photon collection efficiency of -9 dB, or 12.6%. We attribute -3 dB to using a parametric amplifier (paramp) in phase preserving mode [6], -2 dB from infrared filters used on the signal output line, and the rest to a combination of losses in microwave switches, circulators, and connectors. There is also a small amount of added noise from the HEMT amplifier due to the finite gain of the paramp.

EXPERIMENTAL SET-UP

Here we describe the experimental set-up. A schematic is shown in Fig. 4. Measurement pulses are generated through sideband mixing. A custom dual channel 14-bit 1 GS/s arbitrary waveform generator (AWG) generates 20-200 MHz signals which are mixed with a local oscillator (LO) to generate shaped pulses at GHz frequencies. The AWG signal is a superposition of frequencies, one for each measurement resonator, so that the signal sent to the chip consists of four frequency multiplexed measurement pulses. The signal arriving at the chip is mostly reflected by the input capacitor of the bandpass filter, and only a small fraction enters the filter. Each one of the frequency multiplexed pulses is then phase shifted by one of the measurement resonators before leaving the chip through the output port. The small input capacitor

ensures only a small fraction of the phase shifted signal is lost by exiting the chip through the input port. After leaving the chip the signal passes through a series of filters, switches and isolators before it is amplified by a parametric amplifier. The signal is then further amplified by a high mobility electron transistor (HEMT) amplifier and room temperature amplifiers before it is down-mixed to MHz frequencies, digitized and recorded by a custom analog to digital converter (ADC). Digital processing then separates the signal into its frequency components and extracts the phase shifts for each component.

- [1] D. Esteve, M. H. Devoret, and J. M. Martinis, *Phys. Rev. B* **34**, 158 (1986).
- [2] R. Barends, J. Kelly, A. Megrant, D. Sank, E. Jeffrey, Y. Chen, Y. Yin, B. Chiaro, J. Mutus, C. Neill, et al., *Phys. Rev. Lett.* **111**, 080502 (2013).
- [3] Z. Chen, A. Megrant, J. Kelly, R. Barends, J. Bochmann, Y. Chen, B. Chiaro, A. Dunsworth, E. Jeffrey, J. Y. Mutus, et al., *Applied Physics Letters* **104**, 052602 (2014).
- [4] Supplementary information.
- [5] Y. Makhlin, G. Schön, and A. Shnirman, *Rev. Mod. Phys.* **73**, 357 (2001).
- [6] C. M. Caves, *Physical Review D* **26**, 1817 (1982).
- [7] www.linear.com/designtools/software

* These authors contributed equally to this work

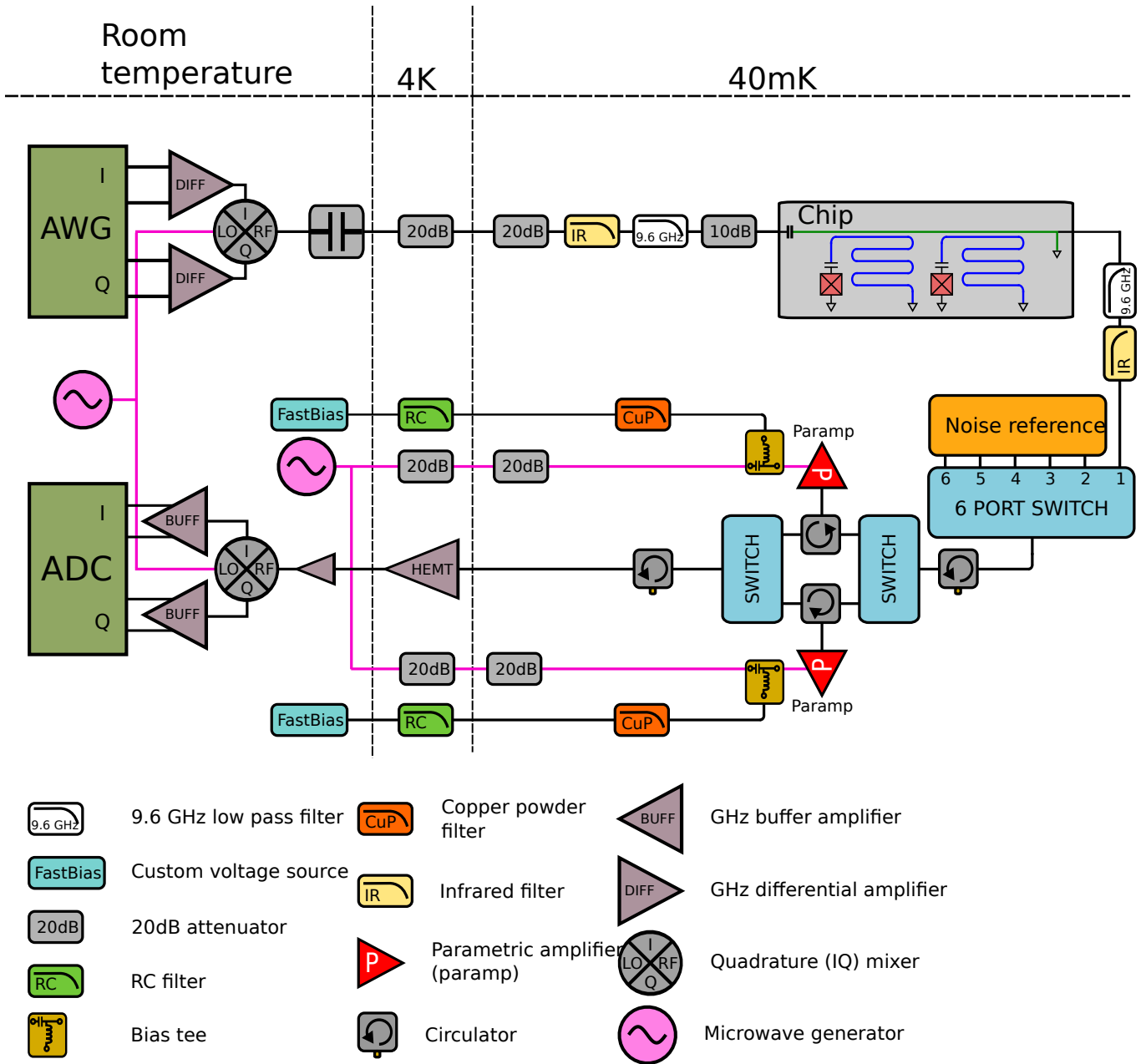


FIG. 4: The experimental set-up. Only components used for state measurement are shown. Pulses are generated by the AWG and mixed to gigahertz frequencies. Cold attenuators, microwave filters, and infra-red filters prevent noise and thermal radiation from reaching the qubits. The transmitted signal is directed through switches to one of two paramps. This allows switching between multiple samples, noise references, and paramps. The signal is further amplified by the HEMT and room temperature amplifiers and digitized. The paramp flux bias is generated by a custom voltage source and filtered by RC and copper powder filters.